Valence-band photoemission study of R_3S_4 (R=La, Ce)

J. -S. Kang,[1] K. Nahm,[2] C. K. Kim,[3] C. G. Olson,[4] J. Pelzl,[5] J. H. Shim,[6] and B. I. Min[6]
[1]*Department of Physics, The Catholic University of Korea, Puchon 422-743, Korea*
[2]*Department of Physics, Yonsei University, Wonju 220-710, Korea*
[3]*Institute of Physics and Applied Physics, Yonsei University, Seoul 120-749, Korea*
[4]*Ames Laboratory, Iowa State University, Ames, Iowa 50011*
[5]*Experimental Physik, Ruhr-University, Bochum D-44780, Germany*
[6]*Department of Physics, Pohang University of Science and Technology, Pohang 790-784, Korea*
(Received 24 September 2001; revised manuscript received 15 April 2002; published 5 August 2002)

Electronic structures of R_3S_4 (R=La, Ce) has been investigated by using photoemission spectroscopy (PES) and electronic structure calculations performed in the LSDA and the LSDA+U method. The valence-band spectrum of La_3S_4 reveals that the electronic states near E_F have mainly La $5d$ character, in agreement with the LSDA calculation. The Ce $4f$ PES spectrum exhibits three prominent features at about -0.5 eV, -2.5 eV, and -5.5 eV. We interpret the Ce $4f$ spectrum as the essentially trivalent Ce $4f$ spectrum, and identify the peaks at -0.5 eV and -2.5 eV as the correlation-split $4f$ states, and the -5.5 eV peak as the hybridized $4f/5d$ states with S p electrons. The CIS and CFS yield spectra show that Ce_3S_4 has formally trivalent Ce^{3+} ions. Nearly half-metallic nature is obtained for ferromagnetic Ce_3S_4, and the LSDA+U calculation provides a reasonably good description of the electronic structure of Ce_3S_4. Superconductivity in La_3S_4 and the absence of the tetragonal distortion in Ce_3S_4 have been discussed based on their electronic structures.

DOI: 10.1103/PhysRevB.66.075108 PACS number(s): 79.60.−i, 71.20.Eh, 71.28.+d

I. INTRODUCTION

The Th_3P_4-type La chalcogenides La_3X_4 (X=S,Se) have attracted much attention because of their high superconducting transition temperatures (T_C=8.3 K for La_3S_4 and T_C=7.4 K for La_3Se_4),[1] and also because of their Jahn-Teller type structural phase transitions at higher temperatures.[2,3] They undergo cubic to tetragonal phase transitions at ~103 K and ~70 K for the stoichiometric La_3S_4 and La_3Se_4 compounds, respectively. The cubic-tetragonal transition temperature T_S shifts to lower values with increasing vacancy concentration x on the La sites in $La_{3-x}X_4$ (X=S,Se).[3] This phenomenon suggests that the structural transition in $La_{3-x}X_4$ depends on the conduction-electron density of states at the Fermi level E_F. La_3S_4 shows a softening in an elastic constant $C'=1/2(C_{11}-C_{12})$ as temperature T is lowered toward T_S,[4,5] which is attributed to itinerant La $5d$ electrons. In the tetragonal phase, a linear-expansion coefficient exhibits an invar-type anomaly with lowering temperature, which has been interpreted as an anomalous lattice expansion driven by conduction electrons and the counteracting normal lattice contraction.[6] In contrast to La_3S_4, no tetragonal distortion has been observed in Ce_3S_4,[3] and the elastic softening is much smaller.[7,8] The ground state of Ce_3S_4 is ferromagnetic with a transition temperature of ~7.2 K.[9]

In spite of extensive investigation on La_3X_4 (X=S,Se), the correlation between the structural and superconducting transitions in La_3X_4 is not well understood yet. The tetragonal structural transition in La_3X_4 has been explained by the band Jahn-Teller mechanism, in which the tetragonal splitting of the La e_g band reduces the free energy.[3,5] The band Jahn-Teller model for La_3S_4 is based on its band structure, which consists of one free-electron-like broad band and a very narrow band with a very high density of states (DOS) at E_F. It has been suggested that the existence of $4f$ electrons in Ce_3S_4 prevents the band Jahn-Teller-type structural transition because the $4f$ level is located at the Fermi level.[8] However, neither the band structure of La_3S_4 nor the $4f$ level in Ce_3S_4 has been confirmed yet. Furthermore, physical properties and the electronic structure of ferromagnetic Ce_3S_4 have not been explored much so far.

Therefore a systematic investigation on the electronic structures of R_3X_4 (R=La,Ce;X=S,Se) is required. In this paper, we have studied electronic structures of Ce_3S_4 and La_3X_4 (X=S,Se) using photoemission spectroscopy (PES). In particular, we have performed resonant photoemission spectroscopy (RPES) measurements near the R $4d\rightarrow 4f$ absorption edge (R=La, Ce). Experimental results are compared to the band-structure calculations of R_3S_4 (R=Ce,La) performed both in the local spin-density approximation (LSDA) and the LSDA+U incorporating the Coulomb correlation interaction U.

II. EXPERIMENTAL AND CALCULATIONAL DETAILS

To prepare stoichiometric La_3Se_4, La_3S_4, and Ce_3S_4, we put S (or Se) in a quartz tube first, and then added La (or Ce) of corresponding quantity. The tube was evacuated and sealed. The temperature of the sealed tube was raised slowly up to 400 °C with an increasing rate of 20 °C/h. In the process, S(Se) and La(Ce) reacted slowly. After this process, temperature was raised to 700 °C and the sample was annealed for 3 days at 700 °C. The reacted sample was ground in the Ar atmosphere and the powder was pressed to form pellet-type samples. La_3S_4 and Ce_3S_4 samples were put into

a Mo crucible and sealed using a plasma arc, whereas La_3Se_4 was put into a W crucible. Next, the Bridgeman-Stockbarger method was employed to obtain single crystals. This process uses a high-temperature oven, over 2300 °C, which is the melting point of these samples. We obtained samples of size in the range of 7 mm diameter and 20 mm height through this process. X-ray powder-diffraction patterns showed a clean single phase with the cubic Th_3P_4 structure for all the samples. In order to determine the vacancy ratio x for the samples, we carried out T-dependent resistivity measurements for $La_{3-x}X_4$ ($X=$S,Se). These results showed that $x \approx 0.016$ for $La_{3-x}S_4$ and $x \approx 0.015$ for $La_{3-x}Se_4$ according to a known interpolation scheme.[3] The vacancy ratio x for $Ce_{3-x}S_4$ has not been determined experimentally, but is expected to be close to that for $La_{3-x}S_4$ ($x \approx 0.016$) because both $La_{3-x}S_4$ and $Ce_{3-x}S_4$ samples were grown in the same way.

Photoemission measurements were done on single crystals[10] of R_3S_4 ($R=$La, Ce) and La_3Se_4 at the Ames/Montana beam line at the Synchrotron Radiation Center (SRC). Samples were fractured and measured in vacuum with a base pressure better than 3×10^{-11} Torr and at T ≈ 15 K. The electron energy analyzer employed in this experiment was a movable 50-mm-radius hemispherical angle-resolved analyzer with two degrees of rotational freedom and an acceptance angle of about 2°. However, the PES spectra obtained from fractured R_3S_4 and La_3Se_4 samples were considered as being angle integrated. This is because the fractured surfaces were not flat microscopically. This argument is supported by the observation that the peak positions in the valence-band PES spectra did not change when the analyzer angle was varied. The Fermi level of the system was determined from the valence-band spectrum of a sputtered Pt foil. The total instrumental resolution (FWHM, full width at half maximum) was about 80 meV at $h\nu \sim 20$ eV and 250 meV at $h\nu \sim 120$ eV All the spectra were normalized to the mesh current.

The electronic structures of R_3S_4 were calculated by employing the self-consistent linearized muffin-tin-orbital (LMTO) band method. The projected angular momentum densities of states (PLDOS's) of La_3S_4 were calculated for the paramagnetic ground state in the LSDA. For Ce_3S_4, the PLDOS's were calculated for the ferromagnetic ground state both in the LSDA and LSDA+U methods. The von Barth-Hedin form of the exchange-correlation potential were utilized. In the LSDA+U method, the spin-orbit interaction is incorporated in the self-consistent variational loop, so that the orbital polarization is properly taken into account.[11]

III. RESULTS AND DISCUSSION

A. Valence-band energy distribution curves

Figure 1(a) presents the normalized valence-band energy distribution curves (EDC's) for Ce_3S_4 in the photon energy ($h\nu$) range of 18–121 eV. Similarly, Figs. 1(b) and 1(c) present the valence-band EDC's for La_3S_4 and La_3Se_4 with 18 eV$\leqslant h\nu \leqslant$117 eV, where the EDC's are scaled at the peak maxima to show their line shapes better. The above $h\nu$ range includes the R $4d$ absorption thresholds ($R=$La, Ce).[12] In Fig. 1(a), $h\nu=121$ and $h\nu=115$ eV correspond to the on- and off-resonance energies due to the Ce $4d\rightarrow4f$ absorption, respectively. Similarly, in Fig. 1(b) and 1(c), $h\nu \approx 117$ eV corresponds to the on-resonance energy in the La $4d\rightarrow4f$ RPES. Therefore the emission enhanced at $h\nu=121$ eV in Ce_3S_4 and that at $h\nu=117$ eV in La_3X_4 ($X=$S,Se) can be identified due to the Ce $4f$ and La $5d$ emission, respectively.

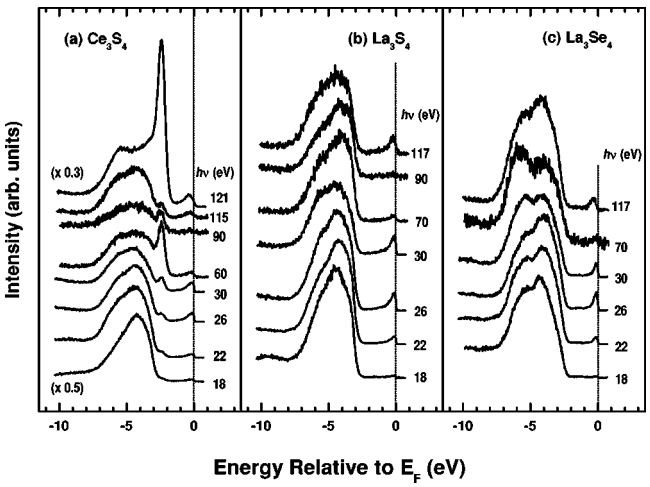

FIG. 1. (a) Valence-band energy distribution curves (EDC's) for Ce_3S_4 for 18 eV $\leqslant h\nu \leqslant$121 eV. Similarly for (b) La_3S_4 and (c) La_3Se_4 for 18 eV $\leqslant h\nu \leqslant$117 eV.

In Ce_3S_4, the off-resonance spectrum at $h\nu=115$ eV is dominated by the S $3p$ emission because at this value of $h\nu$ the Ce $5d$ electron cross section is negligible with respect to the S $3p$ cross section ($\lesssim$1% of the S $3p$ emission[13]) and the Ce $4f$ emission is suppressed at the off-resonance energy due to the interference effect. The latter argument is supported by the fact that the $h\nu=90$ eV spectra well away from the resonance are very alike for Ce_3S_4 and La_3S_4, except for a small bump at ~ -2.5 eV and a peak near E_F for Ce_3S_4 due to the incompletely suppressed Ce f emission (see Fig. 5).[14] At low $h\nu$'s, the relative Ce $5d$ cross section becomes the largest at $h\nu \approx 30$ eV, where it is comparable to the S $3p$ cross section.[13] However, since the Ce $5d$ and S $3p$ states are strongly hybridized to each other, the Ce $5d$ partial spectral weight (PSW) resembles the S $3p$ PSW.

In La_3S_4 and La_3Se_4, the line shape of the valence-band spectrum does not change much with varying $h\nu$, indicating that the La $5d$ and S $3p$ (Se $4p$) states are highly hybridized to each other. In contrast to the strong $4f$ resonance in Ce_3S_4, the magnitude of the $5d$ resonance in La_3X_4 ($X=$S,Se) is very weak. This phenomenon reflects the itinerant character of La $5d$ electrons, as explained below. RPES arises from the interference between the two processes, a direct PES process

$$4d^{10}4f^n5d^m + h\nu \rightarrow 4d^{10}4f^n5d^{m-1}\epsilon_k \qquad (1)$$

and another Auger decay process following a photoabsorption of a core electron to an unoccupied localized state

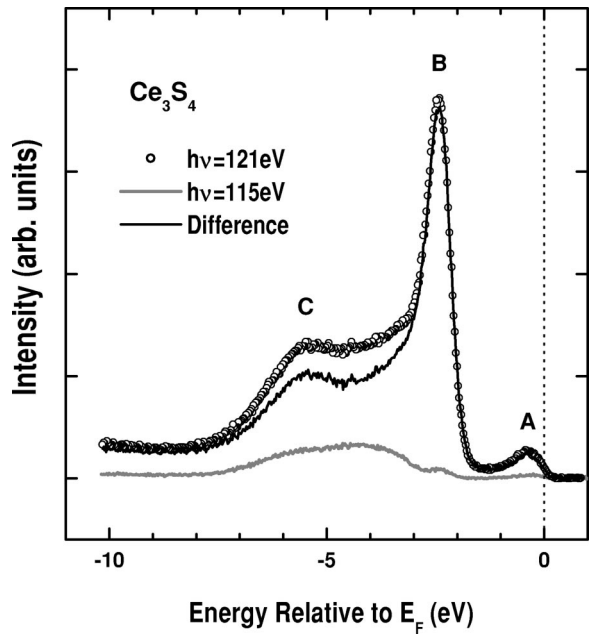

FIG. 2. Normalized valence-band spectra for Ce_3S_4, obtained at the $4d \rightarrow 4f$ on-resonance ($h\nu = 121$ eV, open dots) and off-resonance ($h\nu = 115$ eV, gray line), respectively. The difference curve (solid line) is considered to represent the Ce $4f$ partial spectral weight (PSW) distribution. See the text for the details of the subtraction procedure.

$$4d^{10}4f^n5d^m + h\nu \rightarrow 4d^9 4f^{n+1}5d^m \rightarrow 4d^{10}4f^n5d^{m-1}\epsilon_k . \quad (2)$$

The larger the Auger matrix element of the Coulomb interaction $\langle 4d, \epsilon_k | 1/r_{12} | 4f, 5d \rangle$ is, the stronger the resonance strength will be. Hence the resonance effect is large when the emitted photoelectron originates from a localized state such as the Ce $4f$ state, while it will be weak when the emitted photoelectron originates from an itinerant state such as the La $5d$ state.

Despite a very weak resonance in La_3X_4, the enhanced features at the on-resonance energy ($h\nu = 117$ eV) represent the resonating La $5d$ electrons. Note that the emission near E_F is enhanced at $h\nu = 117$ eV, compared to $h\nu = 90$ eV, where the S $3p$ (Se $4p$) emission is dominant over the La $5d$ emission.[13] The FWHM of the peak near E_F is about 0.5 eV. This behavior indicates that the electronic states near E_F have mainly La $5d$ electron character in La_3X_4, corresponding to an occupied bandwidth of $\lesssim 0.5$ eV.

B. R $4d \rightarrow 4f$ RPES (R = La, Ce)

Figure 2 presents the subtraction procedure of the Ce $4d \rightarrow 4f$ off-resonance spectrum (gray line) from the on-resonance spectrum (dots), and the difference curve (solid line). The difference curve is considered to represent the extracted Ce $4f$ PSW. All the spectra were normalized to the mesh current, as described in Sec. II. No further scaling has been done on the on- and off-resonance spectra before subtraction. Namely, in the extraction of the Ce $4f$ PSW distribution, we have ignored the $h\nu$ dependence of the emission from non-$4f$ valence-band electrons (Ce $5d$ and S $3p$ electrons). This subtraction scheme seems to be reasonable since the line shape of the extracted Ce $4f$ PSW is found to be insensitive to the relative scale factor used for the off-resonance spectrum because of the strong Ce $4f$ resonance.

The difference curve exhibits three prominent features at about -0.5 eV (A), -2.5 eV (B), and -5.5 eV (C). There is some ambiguity in the relative intensity of C in the extraction procedure of the Ce $4f$ PSW, depending on the scale factor multiplied to the off-resonance spectrum to account for the $h\nu$ dependence of conduction-band electrons. In addition, the bulk $4f$ spectrum of Ce_3S_4 might be somewhat different from the difference curve in Fig. 2 because of the large surface $4f$ contribution in the Ce $4d \rightarrow 4f$ RPES region.[15,16] In this context, a more bulk-sensitive Ce $3d \rightarrow 4f$ RPES measurement will be useful.

The peaks A and B are reminiscent of the well-known double-peak structures observed in Ce metal and metallic Ce compounds,[17–20] while the high-binding-energy (BE) peak (C) seems to reflect the hybridization of Ce $4f$ electrons to neighboring valence-band electrons. On the other hand, the Ce $5d$ resonance is known to occur in the Ce $4d \rightarrow 4f$ RPES. To check the contribution from the Ce $5d$ states to the peak C, we have estimated the relative resonance strengths of $5d$ and $4f$ states in Ce_3S_4, assuming that the resonance strength of $5d$ states in Ce_3S_4 is comparable to that in La_3S_4.[21] The estimated resonance strength of the $5d$ states in La_3S_4 is about $\lesssim 20\%$ of the $4f$ resonance Ce_3S_4. This value suggests that the resonating Ce $5d$ states might also contribute to the high-BE peak C in Ce_3S_4 to some extent. Therefore we interpret that the high-BE peak C arises from both the Ce $4f$ and $5d$ states hybridized to neighboring valence-band electrons. The large intensity of the 2.5-eV BE peak (B) and the rather low intensity of the peak near E_F (A) indicate the localized character of Ce f electrons in Ce_3S_4. The origin of the peak near E_F in Ce systems is still controversial.[16–19,22–24] The detailed nature of each peak in the Ce $4f$ PSW of Ce_3S_4 will be discussed later under Figs. 5 and 6.

Note that the nearest-neighbor separation between Ce sites in Ce_3S_4 ($d = 4.03$ Å) (Ref. 3) is larger than the critical Ce-Ce distance in the Hill plot (3.3–3.5 Å),[25] beyond which the Ce $4f$ electrons are observed to form local moments. Thus it is likely that the direct interaction between near-neighbor Ce $4f$ electrons is negligible in Ce_3S_4, and that the interaction between Ce $4f$ electrons should be mediated by the hybridization to neighboring valence-band electrons, such as Ce $5d$ and S $3p$ electrons. The nearest-neighbor separation between Ce and S atoms (2.88 Å) is much shorter than that between Ce and Ce atoms (4.03 Å), suggesting that the Ce $4f$–S $3p$ hybridization is larger than the Ce $4f$–Ce $5d$ hybridization. Therefore we interpret the major origin of peak C (-5.5 eV) in the Ce $4f$ PSW as due to the Ce $4f$–S $3p$ hybridization and/or the Ce $5d$–S $3p$ hybridization.

Figure 3 compares the constant-initial-state (CIS) spectra of R_3S_4 (R = La, Ce) for several initial-state energies E_i

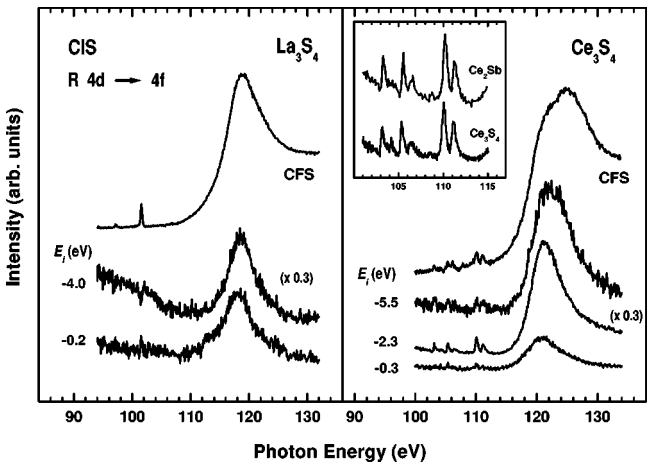

FIG. 3. The constant-initial-state (CIS) spectra of R_3S_4 (R = La, Ce) for several initial-state energies E_i, taken across the R $4d \rightarrow 4f$ absorption thresholds. The top curves are the constant-final-state (CFS) partial yield spectra. Inset: Comparison of the enlarged CIS fine structures of Ce_3S_4 to those of Ce_2Sb (from Ref. 28).

through the valence bands, taken around the R $4d$ absorption thresholds (R=La, Ce). In taking a CIS spectrum, $h\nu$ and E_K are simultaneously varied so as to keep $-E_i = h\nu - \phi - E_K$ constant (E_K, kinetic energy; ϕ, work function). The CIS spectrum measures the RPES cross-section line shape, determined by the initial and final states.[26] The CIS spectra of Ce_3S_4 with $E_i = -0.3$ eV (A), -2.3 eV (B), and -5.5 eV (C) show very strong Fano-type enhancement in the photoionization cross section around $h\nu \sim 121$ eV, indicating that the states at ~ -6 eV$\leqslant E_i \leqslant E_F$ have Ce $4f$ electron character. The similarities of the CIS's for the three initial states show that they have a common origin in the f emission. The CIS spectra of La_3S_4 with $E_i = -0.2$ and -4.0 eV also reveal enhancement at about $h\nu \sim 117$ eV, at the La $4d \rightarrow 4f$ resonance energy in the La $5d$ RPES.[27,28] This finding supports that the electronic states near E_F in La_3S_4 certainly have La $5d$ electron character, which is consistent with the finding in Fig. 1.

On top of the CIS spectra are shown the constant-final-state (CFS) partial yield spectra of R_3S_4 (R=La, Ce). The CFS partial yield spectrum was taken with a kinetic energy E_K of 2 eV. Since the photoelectrons with $E_K = 2$ eV have an estimated electron escape depth of the order of a few tens Å, the CFS partial yield spectrum can be regarded to represent the bulk spectrum of the material and indeed the CFS corresponds to a photoabsorption spectrum. The overall CFS spectrum of Ce_3S_4 is characteristic of trivalent Ce^{3+}, as reported in Ref. 29. The inset compares the enlarged CIS fine structures of Ce_3S_4 to those of the typical trivalent Ce_2Sb. The latter spectrum has been reproduced from the literature.[28] The CIS fine structures at the onset of the Ce $4d$ absorption serve as fingerprints for the valence state of Ce ions. If Ce ions have different valence states, the energy separations and relative strengths among the fine structures in the CIS spectra would be very different. Essentially the same fine structures for Ce_3S_4 and Ce_2Sb indicate that Ce_3S_4 has formally Ce^{3+} ions.

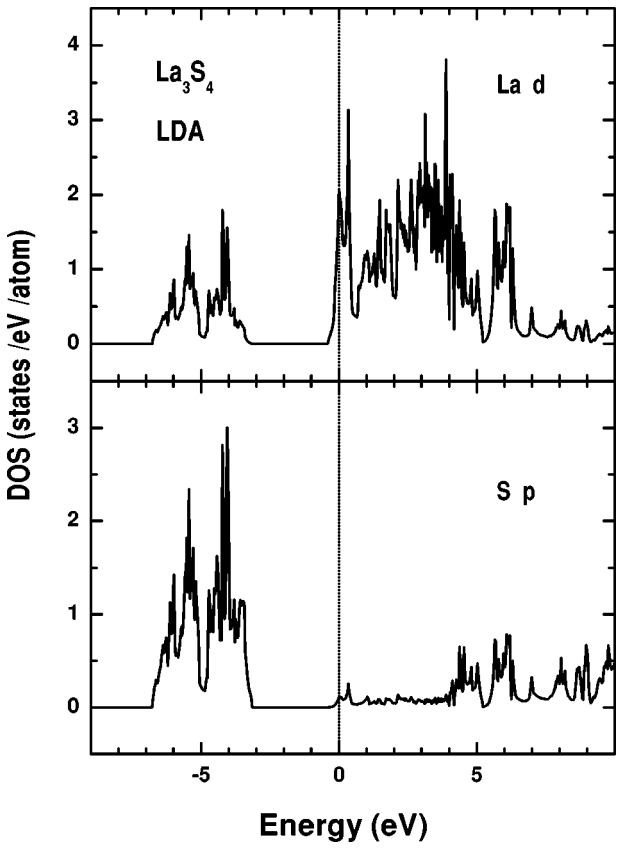

FIG. 4. The projected local density of states (PLDOS) of La d and S p states for La_3S_4, obtained from the LSDA calculation for the paramagnetic ground state.

C. Comparison to the LSDA and LSDA+U calculations

To examine the microscopic origin of the valence-band electronic structures of R_3S_4 (R=La, Ce), we have calculated the electronic structures of R_3S_4 (R=La, Ce) in the LSDA and LSDA+U approximation. Figure 4 shows the La d and S p PLDOS's of tetragonal La_3S_4, obtained from the LSDA calculation by assuming paramagnetic ground state. Each PLDOS is per atom. It is shown that the valence band extends from E_F to about 7 eV below E_F, in agreement with the measured photoemission spectra (see Fig. 1). There is a gap between -0.5 and -3 eV. Most of the occupied La d states are concentrated at -3 to -7 eV and a small occupied DOS peak appears near E_F, corresponding to the tail of the huge unoccupied DOS above E_F. The Fermi level of La_3S_4 is located near a DOS peak, in agreement with the fact that La_3S_4 is a superconductor.[3]

The DOS of cubic La_3S_4 is very similar to that of tetragonal La_3S_4, except that the bands are split and the PLDOS near E_F becomes smeared and a bit wider in the tetragonal structure.[30] Note that the width of the La band near E_F is about 200 meV, which is comparable to the measured width (Fig. 1), but is larger by almost one order than the fitting parameters used in the analysis of the elastic properties of

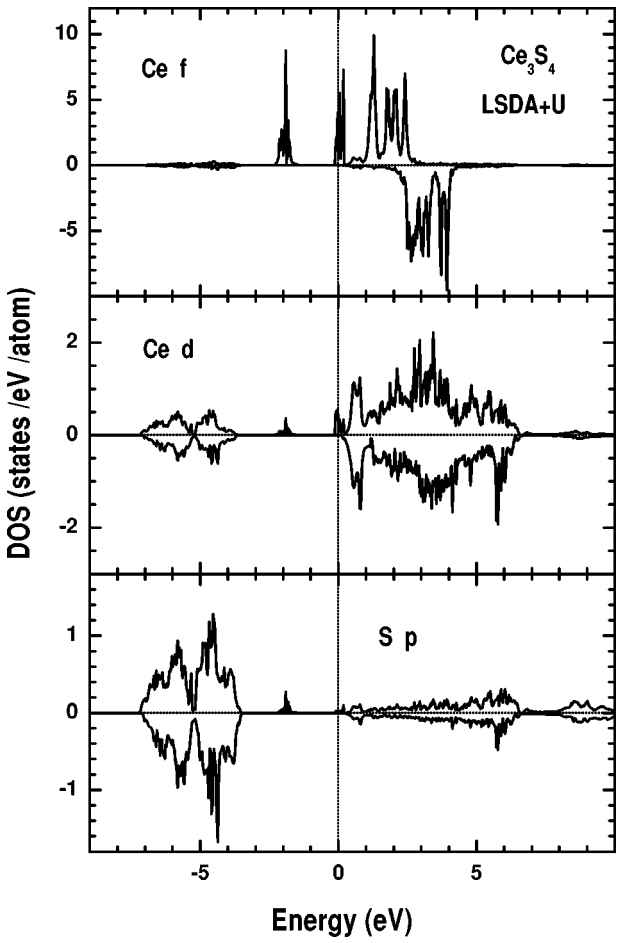

FIG. 5. The PLDOS for Ce_3S_4, obtained from the LSDA+U calculation for the ferromagnetic ground state. From the top, the majority-spin (upper curve) and minority-spin (lower curve) Ce *f*, Ce *d*, and S *p* PLDOS's.

La_3S_4 and Ce_3S_4 in terms of the band Jahn-Teller model.[8]Hence a more refined model that considers the realistic bandwidth of the La e_g band is required. The S *p* bands are nearly filled with a very low DOS at E_F, in agreement with the very low spectral intensity in the S 3*p* PSW [see the $h\nu=18$ eV or $h\nu=90$ eV spectrum in Fig. 1(b)]. Therefore the main contribution to $N(E_F)$ comes from La *d* electrons ($\sim$60%) with a small contribution from S *p* electrons ($\sim$3%). The La *d* and S *p* PLDOS's are very similar each other, indicating large hybridization between the two states. Our theoretical result on La_3S_4 is qualitatively consistent with the previous report.[31]

Figure 5 presents the Ce *f*, Ce *d*, and S *p* PLDOS's of Ce_3S_4, obtained from the LSDA+U calculation by assuming the ferromagnetic ground state. Each PLDOS is per spin and per atom. The parameters used in this calculation are the Coulomb correlation $U=7.0$ eV and the exchange $J=0.98$ eV for the Ce 4*f* electrons. In choosing the U value for Ce_3S_4, we started from the experimental U values for other Ce compounds, and then chose the value which gave reasonably good agreement with the measured PES spectra for Ce_3S_4. It has been known experimentally that the on-site Coulomb interaction energy between Ce 4*f* electrons is $\approx 5-7$ eV.[17,32] The effects of including the on-site Coulomb interaction between the Ce 4*f* orbitals in the LSDA+U are (i) the shift of the occupied 4*f* peak below E_F toward a higher BE and (ii) the shift of the unoccupied 4*f* peak above E_F farther away from E_F. The former effect makes the Ce *f* bands move well below E_F, which were originally concentrated around E_F in the LSDA. The spin-up *f* PLDOS shows the seven split subbands, and the Fermi level lies in the second spin-up Ce *f* subband. The Ce *f* PLDOS exhibits the exchange-split spin-up and -down 4*f* bands, separated by about 2–4 eV from each other. In contrast, the Ce *d* and S *p* PLDOS's exhibit nearly no exchange splitting, indicating that the spin polarization in Ce_3S_4 is mainly due to Ce 4*f* electrons. The calculated spin and orbital magnetic moments for Ce are $1.27\mu_B$ and $2.81\mu_B$, respectively. Since their polarization directions are opposite, the total magnetic moment of Ce becomes $1.54\mu_B$.[33]

The Ce *d* and S *p* PLDOS's of Ce_3S_4 obtained from the LSDA+U calculation are essentially the same as those from the LSDA calculation. The Ce *d* and S *p* PLDOS's share common features, again indicating the large hybridization between them. The difference between Ce_3S_4 and La_3S_4 is that a small peak is observed at about -2 eV in both Ce *d* and S *p* PLDOS's, which reflects the hybridization with Ce *f* electrons. The largest contribution to (E_F) comes from the Ce *f* electrons ($\sim$87%) with a small contribution from Ce *d* electrons ($\sim$10%). Thus our LSDA+U calculation is compatible with the previous suggestion that the existence of 4*f* electrons at E_F prevents the band Jahn-Teller-type structural transition in Ce_3S_4.[8] Note in Fig. 5 that the minority-spin states are negligible at E_F, suggesting that Ce_3S_4 is nearly half-metallic in its ferromagnetic phase. In the half-metallic phase, conduction carriers are 100% spin polarized. The spin-polarized PES experiment is desirable to check this feature.

Figure 6 compares the experimental Ce 4*f* PSW, the $h\nu=26$ eV, and $h\nu=18$ eV spectra of Ce_3S_4 (left) to the calculated Ce 4*f*, Ce 5*d*, and S 3*p* PLDOS's (right) obtained from the LSDA+U calculation. In each theory curve, the region for $E \leqslant E_F$ is shown to represent the occupied part of PLDOS. Then the theory is convoluted with a Gaussian function of 0.2 eV at FWHM to simulate the instrumental resolution. We have not extracted the Ce 5*d* and S 3*p* PSW's because of the large hybridization between them, which makes it difficult to separate out each PSW. Nevertheless, the enhanced emission near E_F at the 5*d* on-resonance ($h\nu=117$ eV) has been identified due to the La 5*d* states in La_3S_4 [Fig. 1(b)], and the Ce 5*d* PSW in Ce_3S_4 is expected to be similar to the La 5*d* PSW in La_3S_4. For Ce_3S_4, the intensity near E_F is the largest at $h\nu\approx 26$ eV (where the relative cross section of Ce 5*d* electrons is the largest), as mentioned in Fig. 1(a). Thus the $h\nu=26$ eV spectrum for Ce_3S_4 is considered to represent a mixture of the Ce 5*d* and S 3*p* PSW's. On the other hand, the S 3*p* emission is expected to be dominant at $h\nu=18$ eV,[13] and so the $h\nu=18$ eV spectrum is considered to represent the S 3*p* PSW.

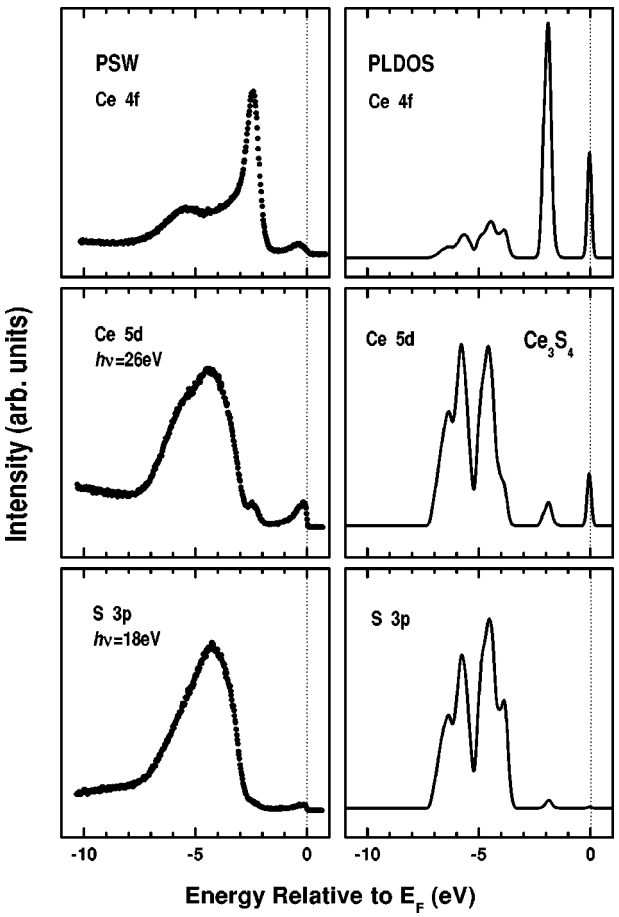

FIG. 6. Left: the experimental Ce $4f$ PSW, the $h\nu=26$ eV, and $h\nu=18$ eV spectra for Ce_3S_4. Right: the calculated Ce $4f$, Ce $5d$, and S $3p$ PLDOS's obtained from the LSDA+U calculation. See the text for details.

It is clearly observed that the trends in the experimental PSW's are in good agreement with those in the LSDA+U calculations. As to the Ce $4f$ states, the main peak around -2.5 eV, a small emission near E_F, and a broad shoulder-like structure around -4 to -6 eV agree well with those in the calculated Ce f PLDOS. The large correlation splitting of Ce $4f$ orbitals in the LSDA+U calculation produces a reasonably good description of the main peak around -2.5 eV in the Ce $4f$ PSW, even though it is still about 0.5 eV off from the experimental position. A larger value of U would yield an improved agreement with the experimental Ce $4f$ PSW. The good agreement between the PES experiment and the LSDA+U calculation for the Ce $4f$ states of Ce_3S_4 is quite surprising, considering the discrepancy found for other metallic Ce systems. In addition, the trend of the higher emission near E_F and the more pronounced -2.5 eV feature in the Ce $5d$ PSW ($h\nu=26$ eV), than in the S $3p$ PSW ($h\nu=18$ eV), is also consistent with the trend in the calculated PLDOS's. Based on the comparison between PES data and theoretical results in Fig. 6, we identify each peak in the Ce $4f$ PSW in Fig. 2: The peak near E_F (A) and the -2.5 eV peak (B) are identified as the split $4f$ states due to the large Coulomb correlation. The -5.5 eV peak (C) arises from the hybridization bonding between Ce $4f/5d$ and S $3p$ states. This interpretation of the Ce $4f$ PSW for Ce_3S_4 awaits the unified picture for the Ce $4f$ spectra of other Ce systems.[17,19]

To summarize, it is found that the LSDA+U calculation provides a reasonably good description of the electronic structure of Ce_3S_4. This finding opens up a possibility that if the on-site Coulomb interaction between Ce $4f$ electrons is properly incorporated in the LSDA band approach, it could describe the electronic structures of some other γ-like Ce compounds. Similarly as in Ce_3S_4, La_3S_4 also shows that the trend in the experimental PSW's (Fig. 1) agree well with those in the LSDA PLDOS's (Fig. 4). This finding is consistent with the previous finding that the La $5d$ states have an itinerant character.

IV. CONCLUSIONS

RPES measurements have been performed on R_3S_4 (R = La, Ce) near the R $4d\rightarrow 4f$ absorption edge, and the measured PSW's are compared to the electronic structure calculations using the LSDA and LSDA+U methods. In contrast to the large Ce $4f$ resonance for Ce_3S_4, a very weak La $5d$ resonance has been observed for La_3X_4 (X=S, Se), reflecting the itinerant character of La $5d$ electrons. The valence-band spectrum of La_3S_4 reveals that the electronic states near E_F have mainly La $5d$ character, which agrees with the LSDA calculation. The extracted Ce $4f$ PSW of Ce_3S_4 exhibits three prominent features at about -0.5 eV, -2.5 eV, and -5.5 eV. By comparing PSW's with the calculated PLDOS's from the LSDA+U, the peak near E_F and the -2.5 eV peak are identified as the correlation-split $4f$ states, and the -5.5 eV peak is identified as the Ce $4f$ states hybridized to S p electrons with some contribution from the Ce $5d$ states. The CFS yield spectrum and the CIS fine structures of Ce_3S_4 are characteristic of trivalent Ce^{3+} ions.

The calculated PLDOS's for R_3S_4 show that most of the occupied La and Ce d states are concentrated at -3 to -7 eV with a small occupied DOS peak near E_F. The La/Ce d and S p PLDOS's share common features, indicating the large hybridization between them. The Fermi level of La_3S_4 is located near a DOS peak, in support of the superconductivity in La_3S_4. Ferromagnetic Ce_3S_4 is found to be nearly half-metallic, and the existence of the f electrons at E_F seems to be consistent with the previous suggestion that the band Jahn-Teller-type structural transition is suppressed due to $4f$ electrons at E_F in Ce_3S_4.

ACKNOWLEDGMENTS

This work was supported by the Center for Strongly Correlated Materials Research (CSCMR) at SNU and the electron Spin Science Center (eSSC) at POSTECH, and in part by the KOSEF-DFG International Collaboration Program (1999). This work is based upon research conducted at the Synchrotron Radiation Center, which was supported by the NSF (contract No. DMR-0084402).

[1] K. Westerholt, H. Bach, R. Wendemuth, and S. Methfessel, Solid State Commun. **31**, 961 (1979).
[2] P.D. Dernier, E. Bucher, and L.P. Longinotti, J. Solid State Chem. **16**, 203 (1975).
[3] K. Westerholt, H. Bach, and S. Methfessel, Solid State Commun. **36**, 431 (1981); K. Westerholt, F. Timmer, and H. Bach, Phys. Rev. B **32**, 2985 (1985). Less than 1% of vacancies on the La sites suppress the tetragonal phase transition completely.
[4] P.J. Ford, W.A. Lambson, A.J. Miller, G.A. Saunders, H. Bach, and S. Methfessel, J. Phys. C **13**, L697 (1980).
[5] C.K. Kim, K. Nahm, Y. Cho, H. Fütterer, and J. Pelzl, J. Phys. F: Met. Phys. **18**, L271 (1988).
[6] R. Pott, G. Güntherodt, W. Wichelhaus, M. Ohl, and H. Bach, Phys. Rev. B **27**, 359 (1983).
[7] H. Fütterer, J. Pelzl, H. Bach, G.A. Saunders, and H.A.A. Sidek, J. Mater. Sci. **23**, 121 (1988).
[8] T.H. Cho, K. Nahm, S.K. You, C.K. Kim, and J. Pelzl, Appl. Phys. A: Mater. Sci. Process. **A70**, 595 (2000).
[9] H. Fütterer, Ph.D. thesis, Ruhr-Universität, Bochum, 1988.
[10] Laue pictures were taken from the fractured samples after PES measurements were over, which confirmed that the measured samples were single crystalline.
[11] S.K. Kwon and B.I. Min, Phys. Rev. Lett. **84**, 3970 (2000).
[12] F. Gerken, A.S. Flodstrom, J. Barth, L.I. Johansson, and C. Kunz, Phys. Scr. **32**, 43 (1985).
[13] J.J. Yeh and I. Lindau, At. Data Nucl. Data Tables **32**, 1 (1985). The photoionization cross sections in actual solids are different from the atomic photoionization cross sections.
[14] The sharp peak at -2.5 eV at the $h\nu=60$ eV spectrum is due to the Ce f electron emission owing to the relatively large Ce f photoionization cross section around $h\nu\sim 50$ eV. See Ref. 13.
[15] L. Duo, Surf. Sci. Rep. **32**, 235 (1998), and references therein.
[16] A. Sekiyama, T. Iwasaki, K. Matsuda, Y. Saitoh, Y. Onuki, and S. Suga, Nature (London) **403**, 398 (2000).
[17] J.W. Allen, S.-J. Oh, O. Gunnarsson, K. Schönhammer, M.B. Maple, M.S. Torikachvili, and I. Lindau, Adv. Phys. **35**, 275 (1987).
[18] B.I. Min, H.J.F. Jansen, T. Oguchi, and A.J. Freeman, Phys. Rev. B **33**, 8005 (1986).
[19] O. Gunnarsson and K. Schönhammer, in *Handbook on the Physics and Chemistry of Rare Earths*, edited by K. A. Gschneidner, L. Eyring, and S. Hüfner (North-Holland, Amsterdam, 1987), Vol. 10, p. 103.
[20] J.-S. Kang, K.C. Kang, and B.I. Min, Physica B **230-232**, 497 (1997).
[21] C.G. Olson, P.J. Benning, M. Schmidt, D.W. Lynch, P. Canfield, and D.M. Wieliczka, Phys. Rev. Lett. **76**, 4265 (1996).
[22] E. Weschke, C. Laubschat, R. Ecker, A. Hohr, M. Domke, G. Kaindl, L. Severin, and B. Johansson, Phys. Rev. Lett. **69**, 1792 (1992).
[23] J.J. Joyce, A.J. Arko, J. Lawrence, P.C. Canfield, Z. Fisk, R.J. Bartlett, and J.D. Thompson, Phys. Rev. Lett. **68**, 236 (1992).
[24] A.B. Andrews, J.J. Joyce, A.J. Arko, J.D. Thompson, J. Tang, J.M. Lawrence, and J.C. Hemminger, Phys. Rev. B **51**, 3277 (1995).
[25] H. H. Hill, in *Plutonium 1970 and Other Actinides*, edited by W. N. Miner, Nuclear Methods Vol. 17 (AIME, New York, 1970), pp. 2–19.
[26] J.-S. Kang, T.W. Noh, C.G. Olson, and B.I. Min, J. Electron Spectrosc. Relat. Phenom. **114-116**, 683 (2001).
[27] J.M. Lawrence, J.W. Allen, S.-J. Oh, and I. Lindau, Phys. Rev. B **26**, 2362 (1982).
[28] C.G. Olson, S.J. Chase, P. Canfield, and D.W. Lynch, J. Electron Spectrosc. Relat. Phenom. **93**, 175 (1998).
[29] G. Kalkowski, C. Laubschat, W.D. Brewer, E.V. Sampathkumaran, M. Domke, and G. Kaindl, Phys. Rev. B **32**, 2717 (1985).
[30] J. H. Shim *et al.* (unpublished).
[31] C. Felser, J. Alloys Compd. **262-263**, 87 (1997).
[32] J.K. Lang, Y. Baer, and P.A. Cox, J. Phys. F: Met. Phys. **11**, 121 (1981).
[33] The experimental value of the magnetic moment is not available.